Combining Radiometric and Spatial Structural Information in a New Metric for Minimal Surface Segmentation

Olivier Nempont, Jamal Atif, Elsa Angelini, and Isabelle Bloch

Ecole Nationale Supérieure des Télécommunications (GET - Télécom Paris)
CNRS UMR 5141 LTCI, Paris, France
{name}@enst.fr⋆

Abstract. Segmentation of anatomical structures via minimal surface extraction using gradient-based metrics is a popular approach, but exhibits some limits in the case of weak or missing contour information. We propose a new framework to define metrics, robust to missing image information. Given an object of interest we combine gray-level information and knowledge about the spatial organization of cerebral structures, into a fuzzy set which is guaranteed to include the object's boundaries. From this set we derive a metric which is used in a minimal surface segmentation framework. We show how this metric leads to improved segmentation of subcortical gray matter structures. Quantitative results on the segmentation of the caudate nucleus in T1 MRI are reported on 18 normal subjects and 6 pathological cases.

Index terms: minimal surface segmentation, level sets, spatial relations, fuzzy knowledge representation.

1 Introduction

Segmentation of structures expressed as a minimal surface extraction problem has been widely discussed in the medical imaging literature. Different optimization methods have been proposed in [1,2,3,4]. Minimal surface segmentation can be performed using geodesic deformable models involving an image-based metric computed from image gradients. An issue arises in the presence of noise and for low contrast structures, such as subcortical gray nuclei in brain magnetic resonance images (MRI), generating weak contour information. To overcome these limitations, some prior information can be incorporated in these methods. For instance, shape priors specific to the structures to segment were introduced in [5] as a non-geodesic additional term in the energy functional constraining the solution to correspond to an admissible shape. Another approach relies on the combination of region and edge information, as for instance in the geodesic active regions introduced in [6].

In this paper, to preserve a strict geodesic formulation, we show how gray levels and structural spatial information can also be efficiently exploited in a metric, and we illustrate this idea on the segmentation of brain internal structures. Indeed, the spatial organization of brain structures is quite stable, and available as prior knowledge. Descriptions of this spatial organization through spatial relations between objects [7,8] were used in [9] to constrain a parametric deformable model, acting as an external force, to segment internal brain structures on normal brains. In [10], this approach was extended to level-set deformable models, in particular using a geodesic formulation. Although the combination of spatial relations information and edge information succeeded in constraining the segmentation to produce acceptable solutions, missing information in the image edge map was not explicitly balanced by the introduction of spatial priors.

We propose a new method to introduce structural information during the metric computation process, in order to obtain a map including complete object boundaries. We first summarize our approach for representing structural information as spatial fuzzy sets in Sect. 2. Our contribution for defining a metric taking into account such information is then detailed in Sect. 3. The integration of this metric into a level-set deformable model formulation is presented in Sect. 4 and applied to the segmentation of subcortical gray nuclei in normal and pathological brain MRI.

2 Representation of Structural Information Using Fuzzy Sets

Fuzzy sets constitute an appealing framework to represent spatial relations, modeling different types of imprecision, related to the imperfections of the image, and to the intrinsic vagueness of some relations [7]. The satisfaction of a given relation is then a matter of degree rather than a "true-or-false" fact. The semantics of spatial relations, which are imprecise but deterministic, is appropriately encoded using fuzzy representations, which then constitute better models than probabilistic ones. Given a relation with respect to a reference fuzzy object A, two types of questions can be formulated:

(i) compute to which degree a target object B fulfills this relation;
(ii) define the points in space where this relation is satisfied.

Formulations of the first type of question have been proposed for a wide range of relations including adjacency, distances, directions and symmetries. In this work, as in [9], we consider the second formulation, based on spatial representations of relations. We do not detail the definitions of the fuzzy sets representations of spatial relations here (see [7] for a review). A spatial relation SR with respect to some reference object is expressed as a fuzzy set in 3D space, with membership function denoted by μ_{SR} (i.e. $\mu_{SR}(x)$ denotes the degree to which a point x satisfies the relation). Most spatial relations can be computed using fuzzy mathematical morphology operations. When several relations are associated to describe the location of an object (as for the caudate nucleus as described below),

the corresponding membership functions are combined using a fusion operator. In the following, μ_{SR} will be used to denote either one relation, or the fusion of several ones.

Spatial relations constitute an important part of the available knowledge about the spatial organization of the brain structures, as evidenced by usual anatomical descriptions, and they remain stable, even in the presence of tumors. In this paper, we rely on the following knowledge:

- for any structure A of the brain, the set $Adj(A)$ of adjacent structures O_i is known, and is assumed to completely surround A;
- the caudate nucleus (CN) is exterior to the lateral ventricle (LV) and close to it. We denote by $\mu_{SR_{CN}}$ the membership function of the spatial fuzzy set representing the fusion of these relations;
- the accumbens nucleus (AN) is located below the lateral ventricle and approximately equidistant from the ventricle and the brain surface; the fuzzy representation of these relations is denoted by $\mu_{SR_{AN}}$.

Note that the computation of $\mu_{SR_{CN}}$ and $\mu_{SR_{AN}}$ is based on a previous segmentation of the lateral ventricles and of the brain surface.

3   Metric Based on Gray-Levels and Spatial Information

Most approaches for minimal surface segmentation rely on low level features such as image gradient. In this section, we illustrate some limits of these approaches and propose to make use of structural knowledge. We derive a generic methodology to include both gray-level and spatial relations in the metric computation.

3.1   Fuzzy Map from Image Gradient

The simplest way to derive a fuzzy edge map μ_I from an image I is to apply an increasing function $g : \mathbb{R}^+ \to [0, 1]$ to the norm of the image gradient. To reduce noise, a Gaussian filter G_σ can be applied, leading to: $\mu_I(x) = g(\|G_\sigma * \nabla I(x)\|)$. Various functions g can be used. As an illustrative example, we use a sigmoid function. This approach does not overcome classical problems related to weak gradients, for instance between the thalamus (Th) and the white matter (WM), as illustrated in Fig. 1 (b).

In [9] a method to enhance weak boundaries was proposed, using the radiometric mean and standard deviation of each type of tissue or structure:

$$\mu_I(x) = g(\|\nabla(p_A(I))(x)\|) = g(\|p'_A(I(x))\nabla(I)(x)\|) \tag{1}$$

where p_A is a Gaussian function defined for each individual structure A. This formula amounts to make g less sensitive to its parameters since it is applied to a contrast-independent representation. Figures 1 (c) and (f) illustrate this fuzzy gradient map for the caudate nucleus. The coronal view shows that there are still parts of the contour missing (cf. red frame).

3.2   Using Region Membership Functions

We propose an alternative method to reinforce the boundary map even in the absence of significant gradients, by using membership functions of the target object and all adjacent structures. Let A be a subset of the spatial domain Ω. The boundary of A may be defined by its morphological gradient: $\partial A = D(A, B_c) \setminus E(A, B_c)$ where D denotes the dilation operator, E the erosion operator, and B_c an elementary structuring element. This definition extends to the fuzzy case: let μ_A be a fuzzy subset of Ω representing object A. The *fuzzy morphological boundary of A* is defined as [11]: $\mu_{\partial A} = \top(D(\mu_A, B_c), D(c(\mu_A), B_c))$, where $\top$ is a t-norm (i.e. a fuzzy conjunction) and c a fuzzy complementation [12].

We can extend this definition to the *boundary between two objects A and B*, with membership functions μ_A and μ_B:

$$\mu_{\partial(A,B)} = \top(D(\mu_A, B_c), D(\mu_B, B_c)).$$

Note that this definition may lead to an empty set. On the other hand it may provide a large fuzzy subset if the objects intersect over a large area.

These definitions require the knowledge of the objects localization, i.e. prior segmentation results defining μ_A and μ_B, which are not yet available. However, from the available knowledge (gray levels, spatial relations...), we can easily obtain fuzzy subsets defining an approximate region of interest for A, denoted by μ_{Gl_A} in case of gray levels information, which is guaranteed to include A.
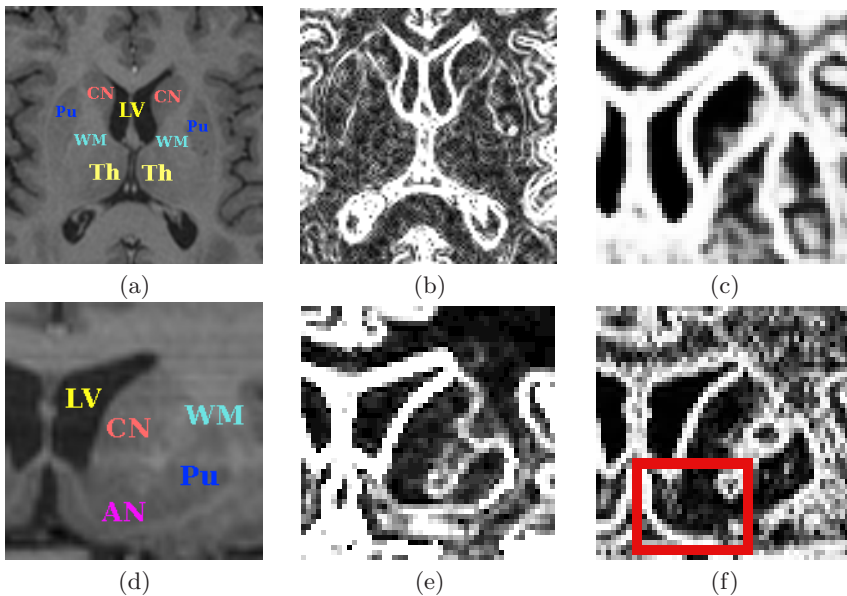
Fig. 1. (a) One axial slice of a brain MRI volume. (b) $\|\nabla I\|$. (c) $g(\|\nabla(p_{CN}(I))\|)$ on an axial view. (d-f) Coronal views.

The fuzzy set μ_{Gl_A} is typically derived from a rough classification performed on the histogram. It does not need to be very accurate and only has to provide an overestimation so as to guarantee the inclusion property $\mu_A \subseteq \mu_{Gl_A}$. The following inclusion property also holds: $\mu_{\partial A} \subseteq D(\mu_{Gl_A}, B_c)$.

The fuzzy subset $D(\mu_{Gl_A}, B_c)$ contains both the object A and its boundaries, and therefore constitutes a poor representation of the object boundaries. To refine this estimation we propose to use prior knowledge about objects adjacent to A, i.e. in $Adj(A)$. Indeed, the boundary of an object A can be expressed as the union of its boundaries with adjacent objects. Since this set is exhaustive, we can write:

$$\mu_{\partial A} = \underset{i}{\perp} \mu_{\partial(A,O_i)} \; , \; O_i \in Adj(A),$$

where $\perp$ is a t-conorm (i.e. a fuzzy union operator). Since we also have ($\mu_A \subseteq \mu_{Gl_A}$ and $\mu_B \subseteq \mu_{Gl_B}$) $\Rightarrow \mu_{\partial(A,B)} \subseteq \top(D(\mu_{Gl_A}, B_c), D(\mu_{Gl_B}, B_c))$, we can derive the following inclusion:

$$\mu_{\partial A} \subseteq \underset{i}{\perp} \top(D(\mu_{Gl_A}, B_c), D(\mu_{Gl_{O_i}}, B_c)), O_i \in Adj(A). \qquad (2)$$

This computational process is illustrated in Fig. 2. Our approach always provides a superset of the boundary, denoted by $\mu_{\partial A}^*$. From prior information on gray levels, we compute the fuzzy subsets $\mu_{Gl_{CN}}$ (b), $\mu_{Gl_{LV}}$ (c) and $\mu_{Gl_{WM}}$ (d) for other structures composed of white matter (WM), to guarantee $\mu_{LV} \subseteq \mu_{Gl_{LV}}$, $\mu_{CN} \subseteq \mu_{Gl_{CN}}$ and $\mu_{WM} \subseteq \mu_{Gl_{WM}}$. From these fuzzy sets we compute a fuzzy set $\mu_{\partial(CN,LV)}^*$ including the boundary $\mu_{\partial(CN,LV)}$ between caudate nucleus and
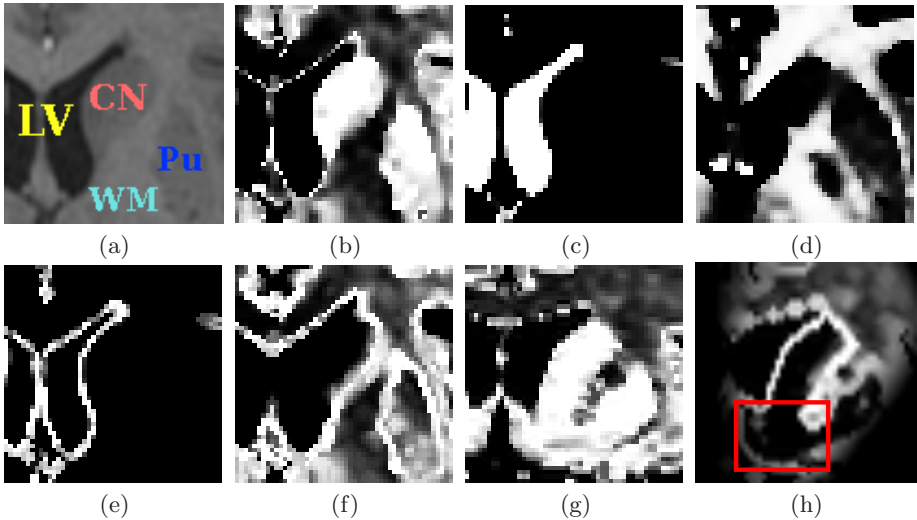
Fig. 2. (a) Zoom on one axial slice. (b) $\mu_{Gl_{CN}}$. (c) $\mu_{Gl_{LV}}$. (d) $\mu_{Gl_{WM}}$. (e) $\mu_{\partial(CN,LV)}^*$. (f) $\mu_{\partial(CN,WM)}^*$. On one coronal slice: (g) $\mu_{Gl_{CN}} = \mu_{Gl_{AN}}$. (h) $\perp(\mu_{\partial(CN,LV)}^*, \mu_{\partial(CN,WM)}^*)$.

lateral ventricle (e), and $\mu^*_{\partial(CN,WM)}$ including the boundary $\mu_{\partial(CN,WM)}$ between caudate nucleus and white matter (f).

While gray-level priors are sufficient to compute an accurate fuzzy subset including the boundary between the caudate nucleus and white matter or lateral ventricle, this is not the case for the accumbens nucleus. Since the caudate nucleus and the accumbens nucleus have similar biological compositions, they cannot be distinguished based on gray levels only (see Fig. 2 (g)). On the other hand considering only the boundary with white matter and lateral ventricle leads to a partial boundary detection, hence having similar drawbacks as gradient based methods (see ROI defined by the red frame in Fig. 2 (h)). Spatial information will allow us to overcome this problem.

## 3.3   Fusion of Fuzzy Edge Maps with Spatial Information

Prior information on the spatial arrangement of structures, as given in a medical knowledge database (see Sect. 2), is of great help to complete missing information in MRI images. In [10], spatial relations represented as fuzzy sets μ_{SR} were merged with boundary information computed by (1) in a conjunctive manner: $\top(\mu_I, \mu_{SR})$. However, as illustrated in Fig. 3, while this fusion operator removes some undesired boundaries, it cannot fill in missing information.

As an alternative approach, we propose to introduce spatial relations, formulated according to the methodology proposed above for fuzzy regions. Since the spatial relations defined for an object A are modeled as regions of interest μ_{SR_A} including the object to be segmented, we always have $\mu_A \subseteq \mu_{SR_A}$. A conjunctive fusion with the fuzzy set representation of gray-level priors is performed so that the property $\mu_A \subseteq \top(\mu_{SR_A}, \mu_{Gl_A})$ is fulfilled. A fuzzy subset including the object boundary is then computed using (2).

In our example this fusion defines a permitted region for the caudate nucleus $\mu^*_{CN} = \top(\mu_{Gl_{CN}}, \mu_{SR_{CN}})$ (Fig. 4 (c)) and one for the accumbens nucleus $\mu^*_{AN} = \top(\mu_{Gl_{AN}}, \mu_{SR_{AN}})$ (Fig. 4 (d)), which allows for a rough discrimination between the two structures. The boundary between the two structures is then computed (Fig. 4 (e)) and combined with the previous results to obtain a fuzzy subset $\mu^*_{\partial CN}$ (Fig. 4 (f)) including the whole boundaries of the caudate nucleus

(a)   (b)   (c)   (d)
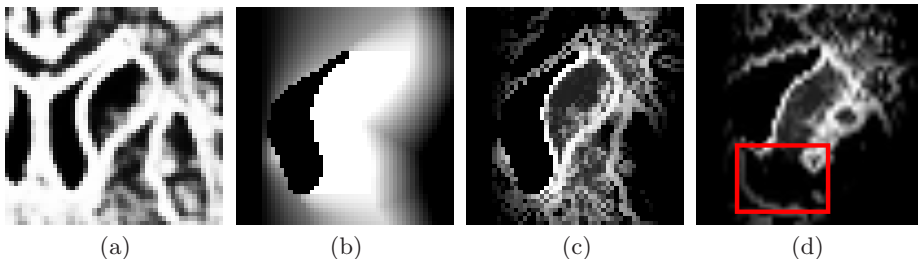
Fig. 3. (a) μ_I computed from (1). (b) $\mu_{SR_{CN}}$. Fusion $\top(\mu_I, \mu_{SR_{CN}})$ on a axial view (c) and a coronal view (d).
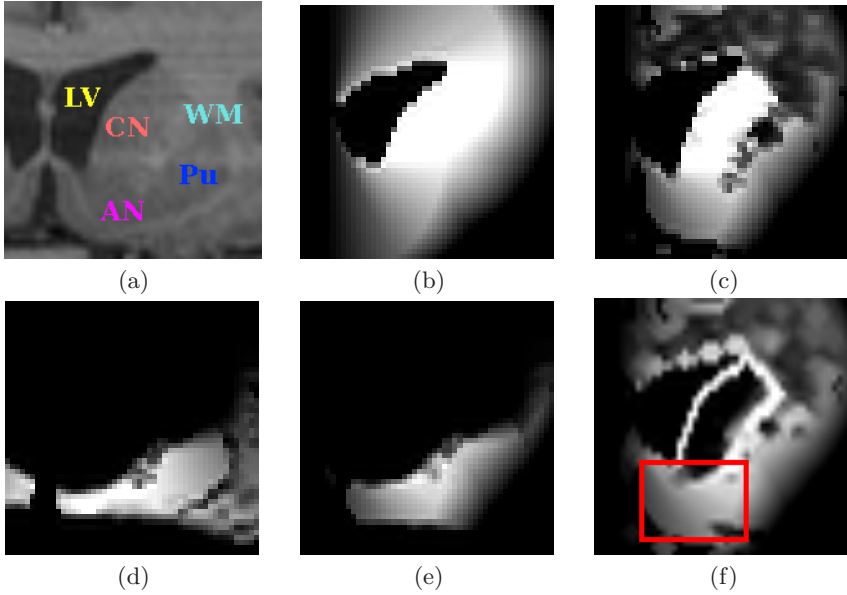
Fig. 4. (a) Zoom on one coronal slice. (b) $\mu_{SR_{CN}}$. (c) $\top(\mu_{SR_{CN}}, \mu_{Gl_{CN}})$. (d) $\top(\mu_{SR_{AN}}, \mu_{Gl_{AN}})$. (e) $\mu_{\partial(CN,AN)}$. (f) $\mu_{\partial CN}$.

$\mu_{\partial CN}$ ($\mu_{\partial CN} \subseteq \mu^*_{\partial CN}$), according to the following equation:

$$\mu^*_{\partial CN} = \bot(\mu^*_{\partial(CN,WM)}, \mu^*_{\partial(CN,LV)}, \mu^*_{\partial(CN,AN)}), \tag{3}$$

with $\mu^*_{\partial(CN,AN)} = \top(D(\mu^*_{CN}, B_c), D(\mu^*_{AN}, B_c))$. The comparison between Fig. 4 (f) and Fig. 3 (d) shows the improvement achieved by the proposed approach. The boundary is now somewhat wide where contour information is missing, but complete, and will be used to constrain the segmentation.

3.4   New Metric Definition

The minimal surface segmentation problem can be expressed as a minimization problem, of an integral formulation involving a metric f_A that should take low values on object boundaries and high values elsewhere. This approach is robust to noise in the sense that high metric values can be compensated by low ones in the integral. Therefore the result may include points corresponding to quite high metric values.

The complementary of the fuzzy set $\mu^*_{\partial A}$ defined by (3) takes low values on object boundaries and therefore could define a suitable metric ($f_A = c(\mu^*_{\partial A})$) to our minimal surface segmentation problem. However, as discussed above, this formulation may lead to solutions for object A whose boundaries contain low values of $\mu^*_{\partial A}$ and thus do not satisfy the key property 2: $\mu_{\partial A} \subseteq \mu^*_{\partial A}$, which ensures that $\mu^*_{\partial A}$ takes high values on all points of ∂A. In order to discard low

values of $\mu^*_{\partial A}$ from the resulting surface, we propose to define the metric as: $f_A = -\log(\mu^*_{\partial A})$, which will strongly disfavor surfaces including points with low values of $\mu^*_{\partial A}$. For numerical purpose, we add an offset to $\mu^*_{\partial A}$, and we define the metric that will be used in the following as:

$$f_A = -\log((1 - \varepsilon)\mu^*_{\partial A} + \varepsilon).$$

4   Level-Set Based Segmentation of Internal Structures of Normal and Pathological Brains

We now describe how the proposed metric can be incorporated in a minimal surface segmentation framework, using a level-set formulation.

4.1   Level-Set Formulation

From the superset of the boundary fuzzy set $\mu^*_{\partial A}$ described above, the minimal surface extraction problem is formulated in the level-set framework as the minimization of the following functional [13]:

$$E(\phi) = \int_\Omega f_A(x)\delta(\phi(x))|\nabla\phi(x)|dx, \tag{4}$$

where ϕ implicitly represents the surface as its zero level and is classically initialized using a signed distance function from an initial shape. The associated Euler-Lagrange equation given by:

$$\frac{\partial \phi}{\partial t} = \delta(\phi)\left(f_A \mathrm{div}\left(\frac{\nabla\phi}{\|\nabla\phi\|}\right) + <\nabla f_A, \nabla\phi>\right) \tag{5}$$

is used to find a local minimum of $E(\phi)$ from an initial surface. The result will thus be strongly dependent on the initial surface. To avoid a convergence towards the empty solution or a weak local minimum, a balloon force can be added.

4.2   Segmentation Protocol

We apply this segmentation method to subcortical gray matter nuclei on MRI brain data. We first extract the brain surface, the lateral ventricles and in pathological cases the tumor [14]. The used methods are robust enough to make the assumption that the resulting segmentations are correct. A Gaussian mixture estimation is performed to obtain gray level fuzzy subsets. Spatial relations are then computed and a boundary map is obtained using (3). This computational framework completely defines $E(\phi)$. The level-set based deformable surface evolution is driven by (5), from an initial shape. This initial shape is obtained automatically by combining spatial relation maps with gray level information. Due to lack of space we do not detail the procedure here but for instance the initialization of the segmentation of the caudate nucleus is based on the following relations: *closed to the body of lateral ventricle, strictly to its right*.

4.3   Data

Segmentation results are evaluated on the caudate nucleus for 18 healty subjects and 6 pathological cases.

The normal database is provided on the Internet Brain Segmentation Repository (IBSR) (http://www.cma.mgh.harvard.edu/ibsr). It contains 18 T1-weighted MR scans ($256 \times 256 \times 128$ volumes, with $1 \times 1 \times 1.5\ mm^3$ resolution). A manual segmentation of 43 structures performed by an expert is also provided and is considered as the ground truth to evaluate our results.

The pathological database is composed of 6 cases illustrated in Fig. 6 affected by brain tumors. The tumors induce various degrees of deformation on the internal nuclei from weak to very large in case of subcortical tumors. The MR scans are $256 \times 256 \times 128$ axial volumes obtained by a SPGR sequence with $0.93 \times 0.93 \times 1.5\ mm^3$ voxel size. Manual segmentation of 8 structures is considered as the ground truth.

4.4   Results

Some results are illustrated in Fig. 5 and 6. The influence of the spatial priors on the segmentation of the lower part of the caudate nucleus is clearly visible on these results. Segmentation accuracy is assessed through comparison with manual segmentations using the following measures:

(i) kappa coefficient: $\frac{2*|A \cap B|}{|A|+|B|}$, which measures agreement between A and B,

(ii) average distance between the surfaces of A (reference) and B (our result),

(iii) Hausdorff distance between A and B.
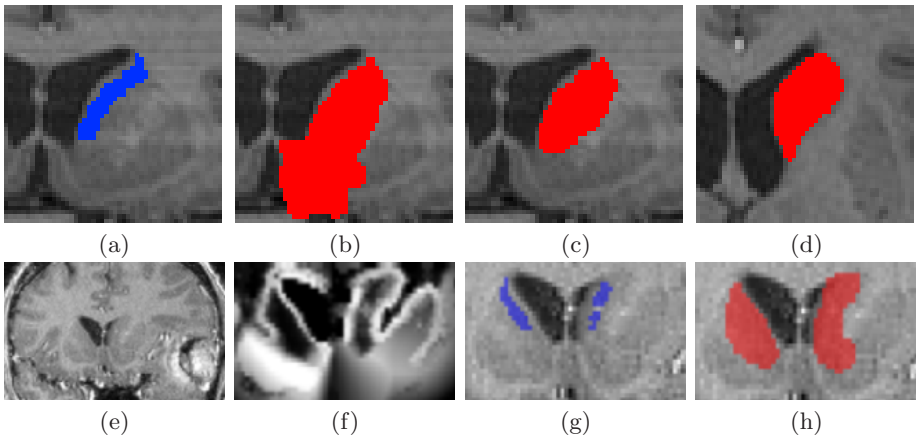
Fig. 5. Segmentation of the caudate nuclei on a normal case. (a) Initialization. (b) Segmentation result without spatial priors. (c, d) Segmentation with spatial priors on a coronal slice and on an axial slice. (e) Coronal slice of a pathological case. (f) $\mu^*_{\partial CN}$. (g) Initialization. (h) Segmentation with spatial priors.
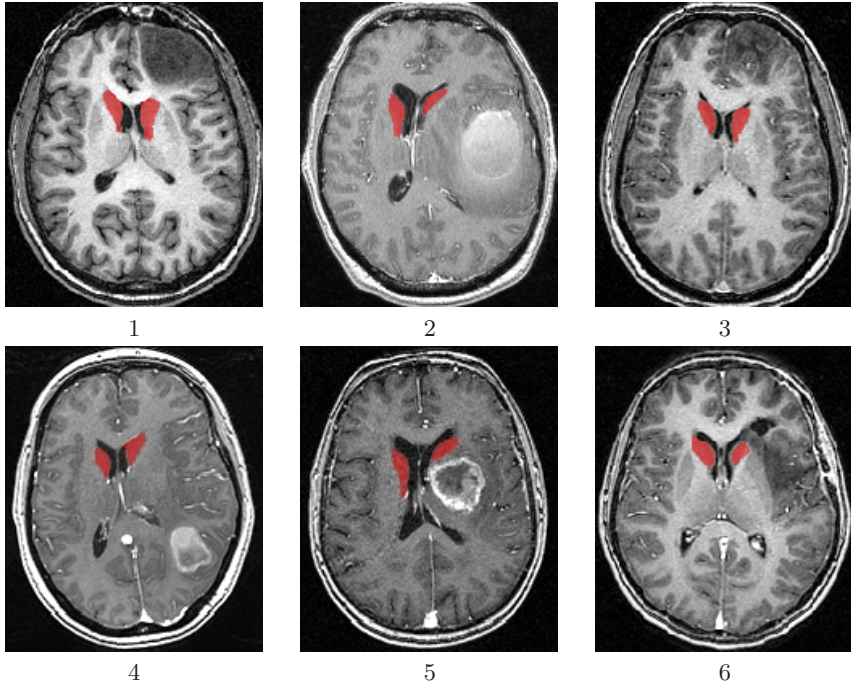
Fig. 6. Axial views of 6 pathological cases. Segmentation results are overlayed in red.

Table 1. Evaluation of the segmentation of the caudate nuclei on IBSR database

Case	Kappa		Average (mm)		Hausdorff (mm)		Case	Kappa		Average (mm)		Hausdorff (mm)	
	left	right	left	right	left	right		left	right	left	right	left	right
1	0.86	0.82	0.68	0.63	6.78	5.74	10	0.82	0.82	0.66	0.57	5.83	5.10
2	0.81	0.85	0.62	0.43	4.90	3.46	11	0.78	0.86	0.61	0.42	5.74	3.46
3	0.80	0.74	0.75	0.81	9.89	4.24	12	0.83	0.84	0.59	0.52	4.90	4.12
4	0.78	0.78	0.77	0.67	5.48	5.48	13	0.82	0.84	0.78	0.59	9.43	5.48
5	0.85	0.85	0.47	0.47	3.00	3.16	14	0.84	0.85	0.50	0.54	3.74	3.74
6	0.83	0.78	0.63	0.96	5.10	7.07	15	0.85	0.85	0.43	0.57	3.00	6.16
7	0.81	0.79	0.50	0.52	4.58	3.61	16	0.83	0.84	0.57	0.69	3.74	5.66
8	0.74	0.74	0.77	0.65	8.54	8.54	17	0.83	0.86	0.77	0.59	6.40	5.74
9	0.82	0.83	0.57	0.52	5.39	6.56	18	0.75	0.75	0.99	1.23	5.48	8.60
							Mean	0.81		0.64		5.50	

Results on normal cases are summarized in Table 1. As an example, results can be compared to those reported in [15] for the same database (where a mean kappa of 0.65 and average distance of $1.71mm$ are reported), or in [16] and [17]

Table 2. Evaluation of the segmentation of the caudate nuclei on pathological cases

Case	Kappa		Average (mm)		Hausdorff (mm)		Case	Kappa		Average (mm)		Hausdorff (mm)	
	left	right	left	right	left	right		left	right	left	right	left	right
1	0.84	0.83	0.67	0.55	10.95	5.83	4	0.75	0.75	0.67	0.72	5.20	9.00
2	0.78	0.85	0.77	0.55	8.06	6.32	5	0.72	0.82	1.58	0.70	19.41	9.11
3	0.80	0.82	0.69	0.55	6.78	5.00	6	0.82	0.85	0.66	0.93	6.17	7.68
							Mean	0.80		0.75		8.29	

for other databases (respectively average distances of $1.60mm$ and $0.60mm$). We can note that the average distance is less than the voxel size (generally $1\times1\times1.5\ mm^3$), and kappa coefficients over 0.7 indicate high agreements between the segmentations [18]. The Hausdorff distance, which corresponds to the worst point, is much more variable, due to imprecise delineation between CN and AN, leading to an arbitrary cut in both manual and automatic segmentations, and thinness of the tail (and also the end of the body) for which minimal surface segmentation is not suited. Results for pathological cases are summarized in Table 2. Among the 12 segmentations, 11 show similar accuracy as in the normal cases. Despite the deformations, spatial knowledge and thus our segmentation framework remain stable. Concerning subject 5, the tumor is adjacent to the left caudate nucleus and induces very large deformations. Improving the results in such cases could rely on an adaptation of the spatial relations, as proposed in [19].

5   Conclusion

The main contribution of this paper is to define a new metric for minimal surface segmentation, incorporating, in a original way, radiometric and structural information. We have shown that missing contour information can be compensated for by exploiting spatial information, based on region gray levels and spatial relations, and how to integrate all these pieces of information in a fuzzy set framework to define metrics for minimal surface extraction. Our approach has been applied, in a geodesic level-set framework, to the segmentation of the caudate nuclei in normal and pathological brain MRI with promising results. Future work aims at extending this approach to other brain structures: while the approach is general, including fuzzy sets have to be specified according to spatial relations specific to each structure.

References

1. Caselles, V., Kimmel, R., Sapiro, G.: Geodesic active contours. In: IEEE International Conference on Computer Vision, ICCV 1995, pp. 694–699 (1995)
2. Boykov, Y., Kolmogorov, V.: Computing geodesics and minimal surfaces via graph cuts. In: IEEE International Conference on Computer Vision, ICCV 2003. pp. 26–33 (2003)
3. Cohen, L., Kimmel, R.: Global Minimum for Active Contour Models: A Minimal Path Approach. International Journal of Computer Vision 24(1), 57–78 (1997)
4. Grady, L.: Computing exact discrete minimal surfaces: Extending and solving the shortest path problem in 3D with application to segmentation. In: IEEE Conference on Computer Vision and Pattern Recognition, CVPR 2006. vol. 1, pp. 69–78 (2006)
5. Leventon, M., Grimson, W., Faugeras, O.: Statistical shape influence in geodesic active contours. In: IEEE Conference on Computer Vision and Pattern Recognition, CVPR 2000. vol. 1, pp. 316–323 (2000)
6. Paragios, N., Deriche, R.: Geodesic active regions: A new framework to deal with frame partition problems in computer vision. Journal of Visual Communication and Image Representation 13(1), 249–268 (2002)
7. Bloch, I.: Fuzzy Spatial Relationships for Image Processing and Interpretation: A Review. Image and Vision Computing 23(2), 89–110 (2005)
8. Bloch, I., Géraud, T., Maître, H.: Representation and Fusion of Heterogeneous Fuzzy Information in the 3D Space for Model-Based Structural Recognition - Application to 3D Brain Imaging. Artificial Intelligence 148, 141–175 (2003)
9. Colliot, O., Camara, O., Bloch, I.: Integration of Fuzzy Spatial Relations in Deformable Models - Application to Brain MRI Segmentation. Pattern Recognition 39, 1401–1414 (2006)
10. Atif, J., Nempont, O., Colliot, O., Angelini, E., Bloch, I.: Level Set Deformable Models Constrained by Fuzzy Spatial Relation. In: Information Processing and Management of Uncertainty in Knowledge-Based Systems, IPMU 2006, pp. 1534–1541 (2006)
11. Bloch, I., Maître, H., Anvari, M.: Fuzzy Adjacency between Image Objects. International Journal of Uncertainty, Fuzziness and Knowledge-Based Systems 5(6), 615–653 (1997)
12. Dubois, D., Prade, H.: Fuzzy Sets and Systems: Theory and Applications. Academic Press, New-York (1980)
13. Gout, C., Le Guyader, C., Vese, L.: Segmentation under geometrical conditions using geodesic active contours and interpolation using level set methods. Numerical Algorithms 39(1), 155–173 (2005)
14. Khotanlou, H., Colliot, O., Bloch, I.: Automatic Brain Tumor Segmentation using Symmetry Analysis and Deformable Models. In: International Conference on Advances in Pattern Recognition, ICAPR 2007, pp. 198–202 (2007)
15. Ciofolo, C., Barillot, C.: Brain Segmentation with Competitive Level Sets and Fuzzy Control. In: Christensen, G.E., Sonka, M. (eds.) IPMI 2005. LNCS, vol. 3565, pp. 333–344. Springer, Heidelberg (2005)
16. Pitiot, A., Delingette, H., Thompson, P., Ayache, N.: Expert knowledge-guided segmentation system for brain MRI. Neuroimage 23(1), 85–96 (2004)
17. Xue, J., Ruan, S., Moretti, B., Revenu, M., Bloyet, D.: Knowledge-based segmentation and labeling of brain structures from MRI images. Pattern Recognition Letters 22(3), 395–405 (2001)

18. Zijdenbos, A., Dawant, B., Margolin, R.: Morphometric analysis of white matter lesions in MR images: method and validation. IEEE Transactions on Medical Imaging 13(4), 716–724 (1994)
19. Atif, J., Hudelot, C., Fouquier, G., Bloch, I., Angelini, E.: From Generic Knowledge to Specific Reasoning for Medical Image Interpretation using Graph-based Representations. In: International Joint Conference on Artificial Intelligence, IJCAI 2007, pp. 224–229 (2007)